PERGAMON

Journal of Structural Geology 22 (2000) 1747–1759

JOURNAL OF STRUCTURAL GEOLOGY

www.elsevier.nl/locate/jstrugeo

Crystallographic and magnetic preferred orientation of hematite in banded iron ores

Heinrich Siemes[a,*], Helmut Schaeben[b], Carlos A. Rosière[c], Horst Quade[d]

[a]*Institut für Mineralogie und Lagerstättenlehre, RWTH-Aachen, Wüllnerstr. 2, D-52056 Aachen, Germany*
[b]*Institut für Geologie, Mathematische Geologie und Geoinformatik, TU Bergakademie Freiberg, Gustav-Zeuner-Str. 12, D-09596 Freiberg, Germany*
[c]*Instituto de Geociências, Universidade Federal de Minas Gerais, Av. Antônio Carlos 6627, Belo Horizonte CEP-31270-901, Minas Gerais, Brazil*
[d]*Institut für Geologie und Paläontologie, TU Clausthal, Leibnizstr. 10, D-38678 Clausthal-Zellerfeld, Germany*

Received 26 November 1999; accepted 21 June 2000

Abstract

The crystallographic preferred orientation of hematite in banded iron ores and the orientation of both the measured and the calculated principal susceptibility axes are strongly related. The maximum susceptibility is aligned with the lineation and the pole of the foliation coincides with the minimum susceptibility, although there are often distinct differences between the measured and calculated values of the susceptibilities. A wide variety of configurations of c-axis pole figures modeled by varying the parameters of the Bingham distribution and Bingham–Mardia-distribution reveal that quite different c-axis patterns of hematite ores may have the same anisotropy of the magnetic susceptibility (AMS) parameters. Large deviations between calculated and experimental AMS-data should initiate further investigations to resolve a probably unnoticed heterogeneity of the fabric. The present investigations show that the structural analysis of the preferred orientation of hematite ores by means of the rather inexpensive and fast magnetic method must be accompanied by the more expensive but unambiguous determination of preferred orientation by x-ray and neutron diffraction experiments in order to accomplish a complete and sound interpretation.

1. Introduction

The relationship between the c-axis fabric of hematite ores measured by means of optical and X-ray-methods and their magnetic fabric measured by means of a torque magnetometer was investigated and described by Hrouda et al. (1985). Since then the preferred orientation of a large series of different hematite ores from several localities and different metamorphic terrains of the Quadrilátero Ferrífero, Minas Gerais (Dorr, 1969) (Fig. 1) was measured by means of neutron diffraction (Brokmeier, 1989; Will et al., 1989) and the magnetic fabric by means of the Kappabridge KLY-2 of the same specimens. Three typical examples are presented in Fig. 2, which are interpreted as c-axis preferred orientations with a rotational degree of freedom of the a-axes around the *c*-axis (Siemes and Hennig-Michaeli, 1985; Will et al. 1990; Wenk, 1998). The minimum susceptibility is located in the center of the *c*-axis maximum, the maximum susceptibility in the center of the (110)-maximum or in the center of (100)-maximum (not shown in Fig. 2). The relationship between the crystallographic preferred orientation and the microfabric is described in Rosière et al. (1998, 1999) and Quade et al. (2000). The abundance of recently acquired data initiated this new analysis of the relationship between the measured anisotrophy of the magnetic susceptibility (AMS)-data, the neutron measured pole figures, and AMS-data calculated from the (003)-pole figures.

2. Calculation and presentation of AMS-data

The AMS of hematite single crystals is characterized by a very small susceptibility K_c parallel to the *c*-axis and a much larger and isotropic susceptibility K_{ab} in the basal plane resulting in a ratio of $P_c = K_{ab}/K_c > 100$ (Hrouda, 1980). In this case the anisotropy is controlled only by the intensity of the c-axis orientation; for example, at a constant *c*-axis concentration, $P_c = 100$, $P_c = 1000$, and $P_c = 10\,000$ give rise to virtually the same values of ore anisotropy degree. In accordance with Hrouda et al. (1985) the values $K_c = 1.0$, $K_a = K_b = 10\,000.0$ were used for the AMS-calculations. These values yield the mean susceptibility of $K_{mean} = 6667.0$, and the relative susceptibilities $K_{arel} = K_{brel} = 1.499925$ (approximately 1.5), $K_{crel} = 1.499925 \times 10^{-4}$ (approximately

* Corresponding author.
E-mail address: siemes@rwth-aachen.de (H. Siemes).

0191-8141/00/$ - see front matter
PII: S0191-8141(00)00085-7

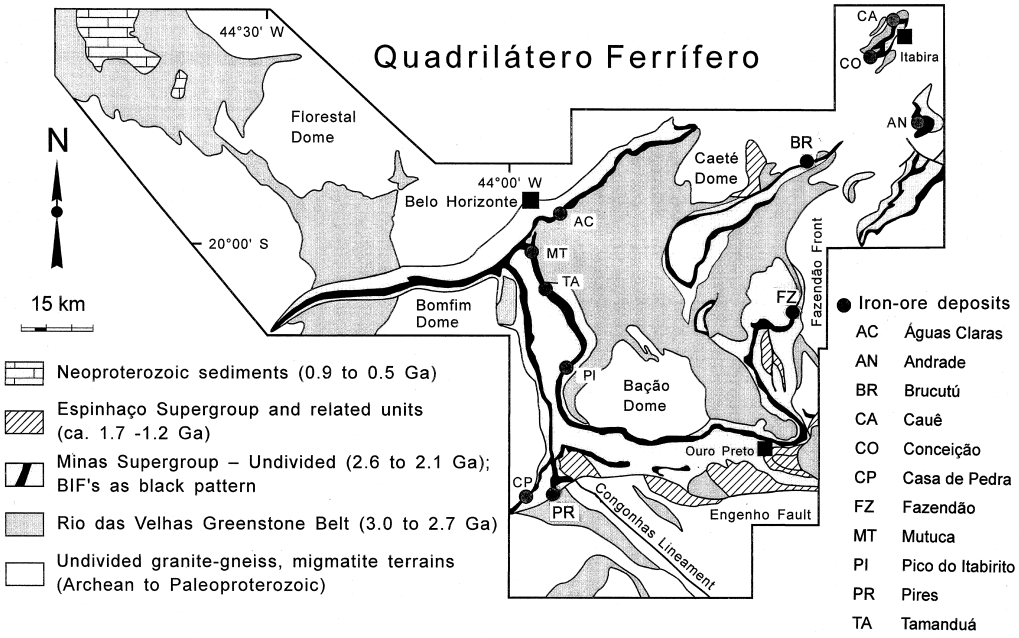

Fig. 1. Geologic Map of the Quadrilátero Ferrífero (modified after Baars and Rosière, 1994) showing locations of the major iron ore mines.

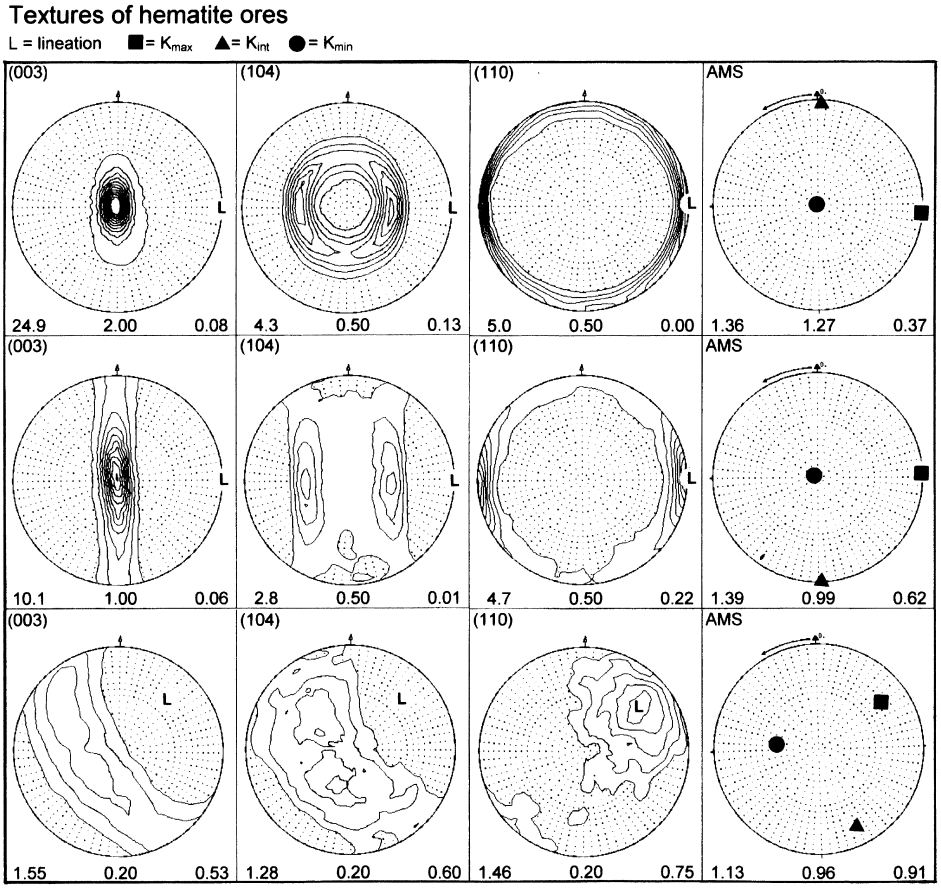

Fig. 2. (003), {104} and {110} pole figures of iron ores from the Quadrilátero Ferrífero and position of principal susceptibility axes. First and second row example from Andrade Mine, third row from Tamanduá Mine. Below the pole figures are indicated in mrd the maximum density, the contour increment and the minimum density, the first contour line is always 1.0 mrd.

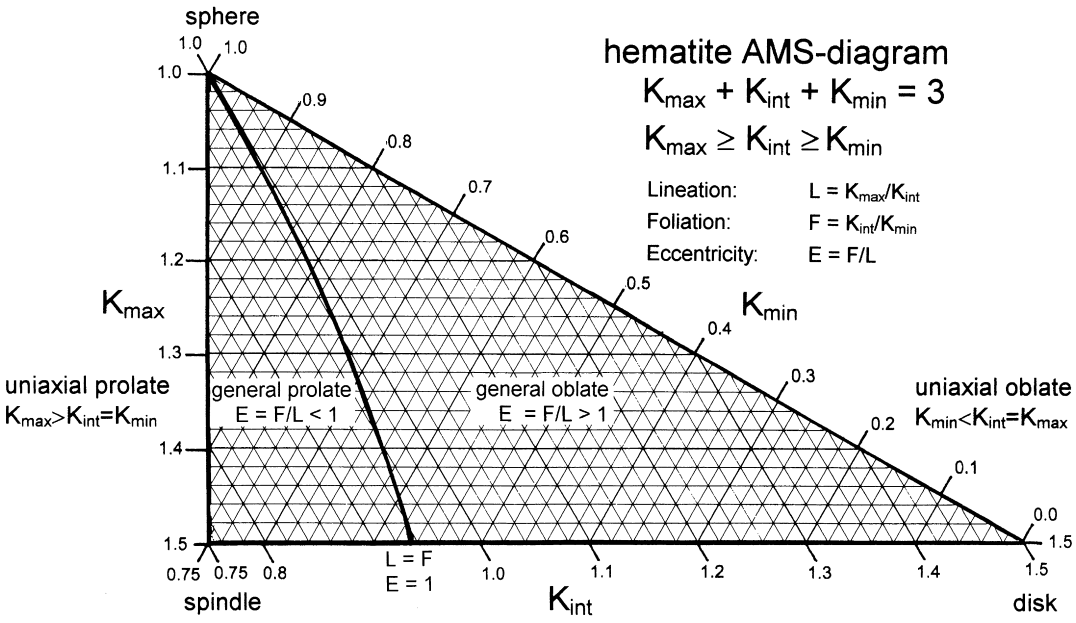

Fig. 3. AMS-diagram of hematite indicating the shape of the susceptibility ellipsoids. L = lineation, F = foliation, $E = F/L$.

0.0). Because of the constraint that the sum of the relative susceptibilities is 3.0 and $K_{max} \geq K_{int} \geq K_{min}$ the measured and calculated AMS-data can be easily visualized in a triangle diagram (Fig. 3) similar to the triangle plot of eigenvalues (Woodcock, 1977). Different parameters and the shape of the ellipsoid can be read from the plotted data points within this AMS-diagram. At the corners of the AMS-diagram the shapes of the susceptibility ellipsoids are indicated. $K_{max} = K_{int} = K_{min} = 1.0$ yields a sphere, $K_{max} = 1.5$ and $K_{int} = K_{min} = 0.75$ a spindle and $K_{max} = K_{int} = 1.5$ and $K_{min} = 0.0$ a disk-like ellipsoid. This disk-shaped ellipsoid has exactly the K-values of the single crystal of hematite. Along the K_{max}-boundary ellipsoids are uniaxially prolate and along the K_{min}-boundary they are uniaxially oblate. Within the diagram the shape of the ellipsoids changes from general prolate to general oblate. The parameters L (magnetic lineation), F (magnetic foliation), E (ratio F to L), P' (magnetic anisotropy), and T (magnetic shape factor) recommended as standard parameters by Ellwood et al. 1988 (Table 1) were calculated from the principal magnetic susceptibilities K_{max}, K_{int} and K_{min}. Fig. 4(a) shows the plot of a few contour lines of the lineation and foliation within the AMS-diagram. In the right field with $F > L$ ($E > 1$) the ellipsoids are oblate, in the left field with $F < L$ ($E < 1$) the ellipsoids are prolate. The boundary between both fields is defined by $F = L$ ($E = 1$). As an example Fig. 4(b) presents contour lines for the parameter P' describing the degree of anisotropy and contour lines of the shape factor T.

3. Numerical simulation of the *c*-axis distribution

In order to get a deeper insight into the relationship between the preferred orientation of hematite and its magnetic fabric a wide range of simulated c-axis distributions was

Table 1
Selected AMS parameters

Principal susceptibilities of a sample	$K_{max} \geq K_{int} \geq K_{min}$
Magnetic lineation[a]	$L = K_{max}/K_{int}$
Magnetic foliation[b]	$F = K_{int}/K_{min}$
Ratio F to L[c]	$E = F/L$
	$E > 1$ oblate susceptibility ellipsoid
	$E < 1$ prolate susceptibility ellipsoid
Shape factor[d]	$T = 2 \times [\ln(K_{int})-\ln(K_{min})]/[\ln(K_{max})-\ln(K_{min})]-1.0$
Degree of anisotropy[d]	$P' = \exp\{\sqrt{[2 \times ((\ln(K_{max})-\ln(K_{mean}))^2 + (\ln(K_{int})-\ln(K_{mean}))^2 + (\ln(K_{min})-\ln(K_{mean}))^2)]}\}$

[a] Balsley and Buddington, 1960
[b] Stacey et al., 1960
[c] Hrouda, 1982
[d] Jelínek, 1981

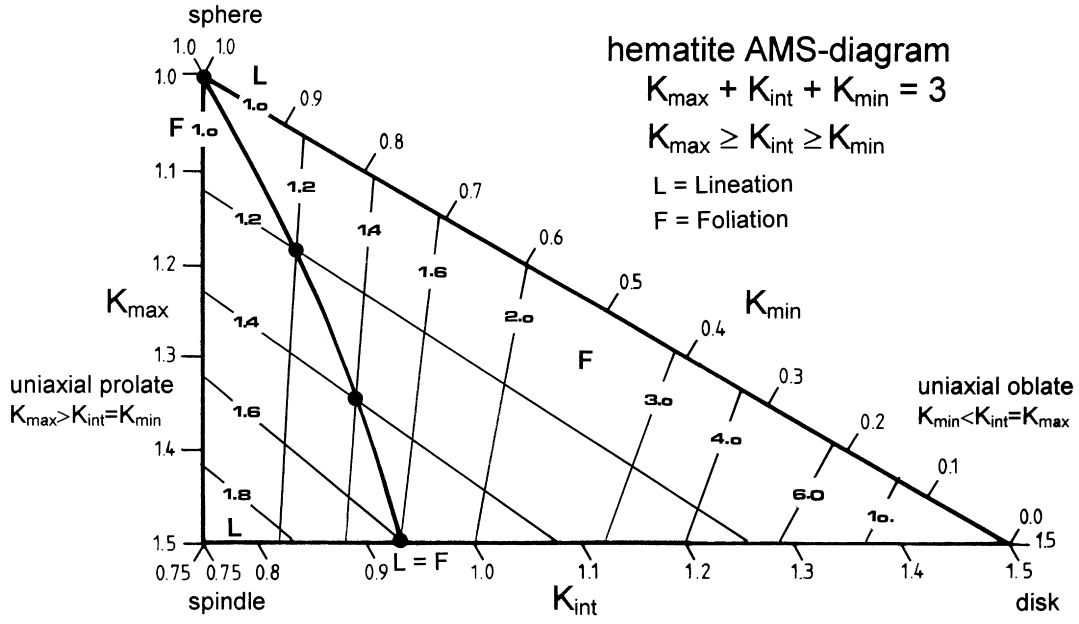

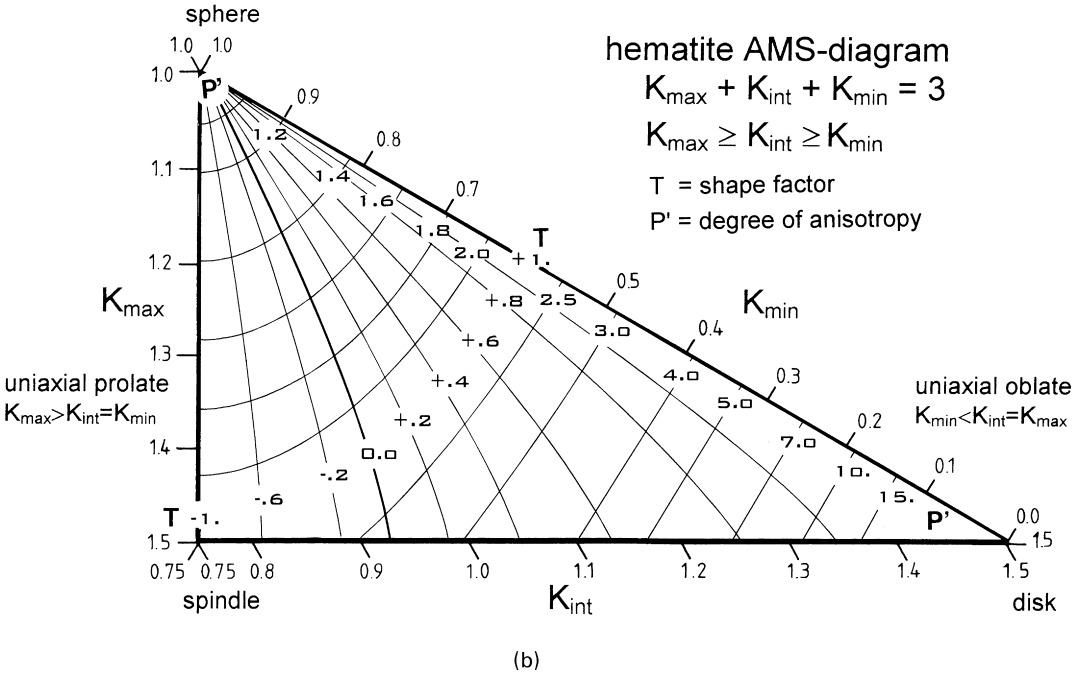

Fig. 4. AMS diagrams of hematite. (a) Contour lines of magnetic lineation L and foliation F. The line $F = L$ indicates the transition between the fields of the oblate and prolate susceptibility ellipsoids. (b) Contour lines of the degree of anisotropy P' and contour lines of the shape factor T.

evaluated. These mathematical c-axis pole figures were generated by a computer code featuring the versatile Bingham (1974) and Bingham and Mardia (1978) distribution, respectively. Both distributions are controlled by location and shape parameters (for details see Appendices A and B).

For a series of mathematical Bingham-distributions the location parameters were kept constant and the shape parameters were systematically varied. The second shape parameter z_2 was set to 25, 10, 5, and 0.5. The ratio of the second shape parameter z_2 to the first z_1 was set to 0.0, 0.5, 0.75, 0.95, and 1.0. The mathematical pole figures presented in Fig. 5(a) are quite similar to the ones found in nature (Rosière et al., 1998, 1999; Quade et al., 2000). The related K-value positions in the AMS-diagram are given in Fig. 5(b). Along the K_{min}-boundary the pole figures reveal circular maxima ($z_2/z_1 = 1.0$) corresponding to uniaxial oblate ellipsoids, and along the K_{max}-boundary pole figures depict

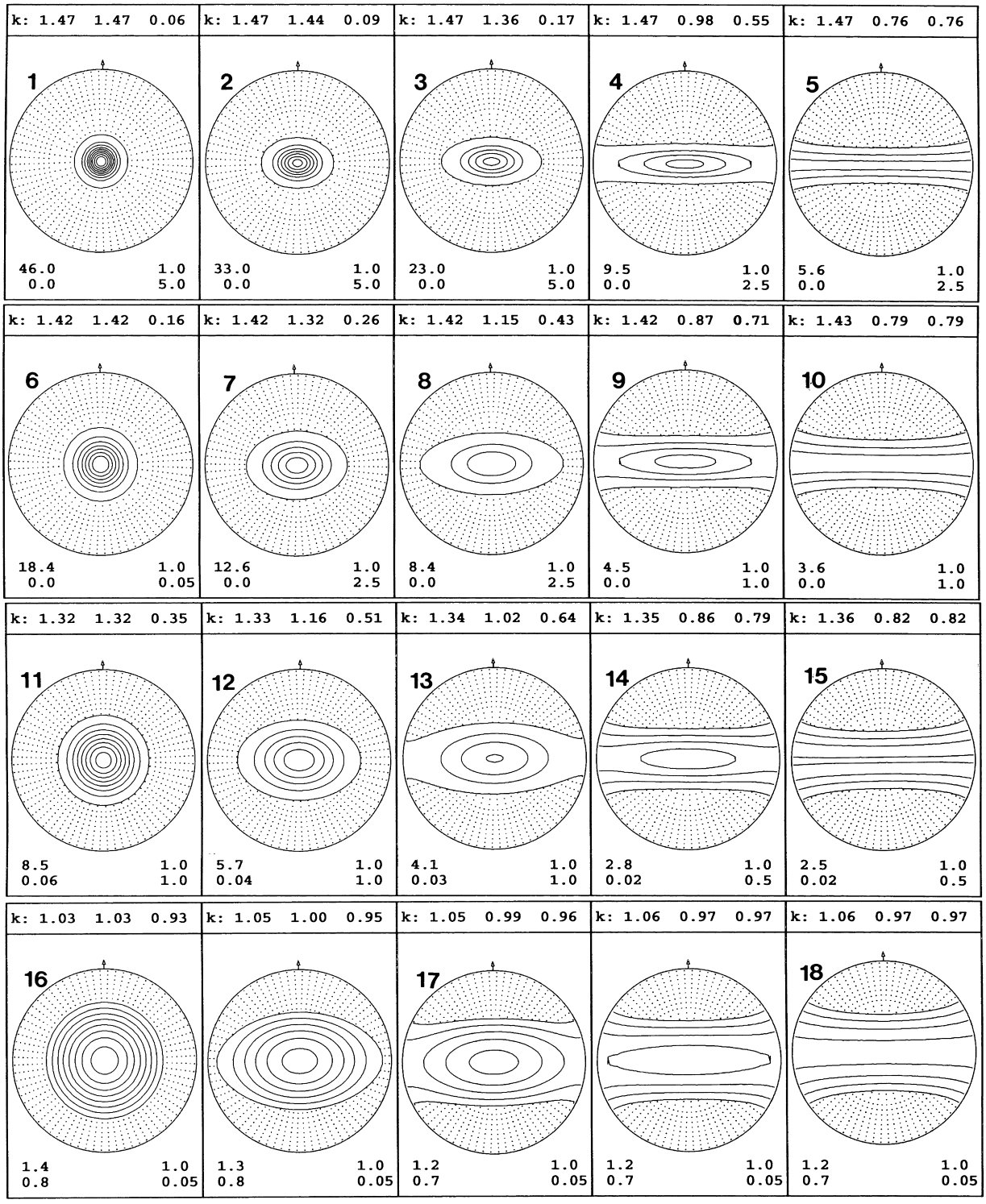

(a)

Fig. 5. Basal plane pole figures mathematically modeled by varying the parameters of the Bingham distribution. In each figure the susceptibilities are indicated on the top line, in the lower left corner the maximum and minimum density, and in the lower right corner the first contour line in mrd and the contour line interval. (a) Pole figures no. 1–5: $z_1 = 25$, $z_2 = 0.0, 12.5, 18.75, 23.75, 25.0$; figures no. 6–10: $z_1 = 10.0$, $z_2 = 0.0, 5.0, 7.5, 9.5, 10.0$; figures no. 11–15: $z_1 = 5.0$, $z_2 = 0.0, 2.5, 3.75, 4.75, 5.0$; figures no. 16–20: $z_1 = 0.5$, $z_2 = 0.0, 0.25, 0.375, 0.475, 0.5$. (b) Location of the mathematical Bingham pole figures in the AMS-diagram.

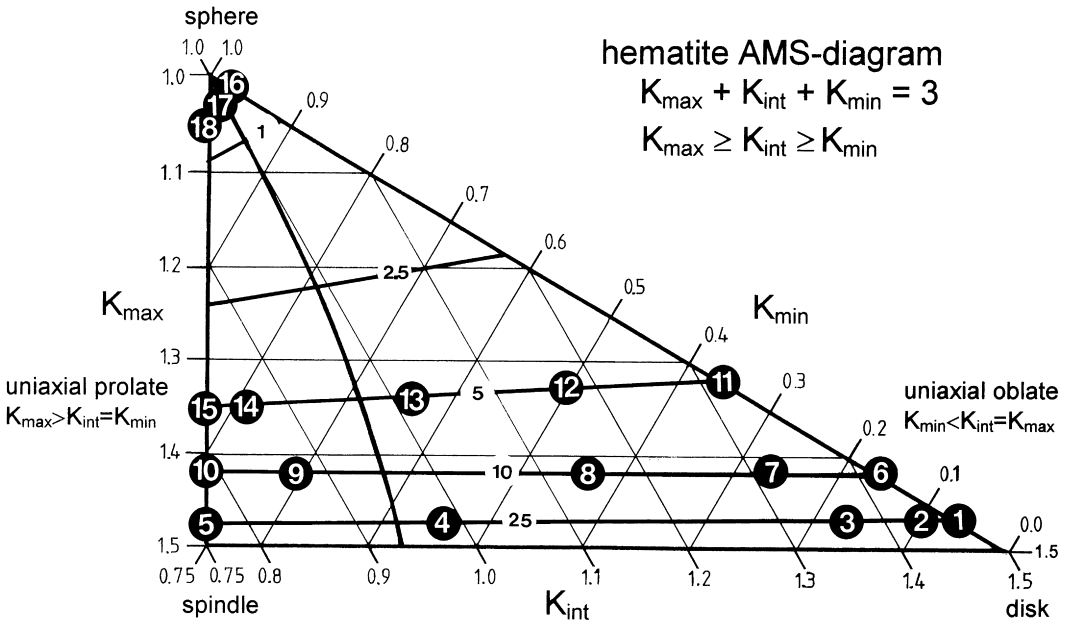

(b)

Fig. 5. (*continued*)

great circle configurations ($z_2/z_1 = 0.0$) corresponding to uniaxial prolate ellipsoids. Within the AMS-triangle the pole figures continuously change from circular maxima, to elliptical maxima, great circles with an elliptical maximum, and pure great circle configurations. In the general cases the axis of the minimum susceptibility is centered at the *c*-axis maximum and the axis of maximum susceptibility is perpendicular to the elliptical *c*-axis maximum or great circle. In the special cases of axisymmetric *c*-axis maxima or perfect great circle configurations only the position of the minimum susceptibility in the center of the maximum resp. the maximum susceptibility perpendicular to the *c*-axis great circle is defined.

The modeled pole figures of Fig. 6(a) with various parameters of the Bingham–Mardia distribution display small circle configurations. Their positions in the AMS-diagram are presented in Fig. 6(b). The calculated susceptibilities for a distribution concentrated around a small circle about 55° apart from the *z*-axis are $K_{max} = K_{int} = K_{min} = 1.0$ that indicates a uniform distribution of the susceptibilities. If the angle of aperture is greater than 55° the maximum susceptibility in the center of the projection corresponds to a great circle distribution of the *c*-axes and if the angle of aperture is smaller than 55° the minimum in the center corresponds to a central maximum. Fortunately these configurations of *c*-axes on small circles are not realistic for hematite ores. The same holds for four of the five pole figures in Fig. 7 where the principal susceptibilities indicate for all of them a random or uniform distribution of the susceptibilities and the *c*-axes.

In Fig. 8(a) in the upper row four superposed pole figures consisting of one great circle configuration with two maxima are presented. The maxima have the same shape parameters, but different location parameters with the maxima 0, 30, 60 and 90° apart. The values of K_{max} remain constant while K_{int} and K_{min} are allowed to vary, but the positions of the axes of the principal susceptibilities remain identical. The pole figures in Fig. 8(a) in the lower row are modeled with single Bingham distributions that generate the same susceptibilities and identical positions in the AMS-diagram (Fig. 8b). This means that very different *c*-axis pole figures cannot be distinguished from each other by means of their AMS anisotropies.

4. Numerical modeling of *c*-axis pole figures

The AMS-diagram of Fig. 9(a) shows the principal susceptibilities measured for 44 naturally deformed samples from 10 different mines at the Quadrilátero Ferrífero, Minas Gerais, Brazil, located at different tectonic settings (Rosière and Chemale Jr., 1991), while Fig. 9(b) depicts the values calculated from the basal pole figures of the same samples. Obviously there are differences between them. Three sample points are numbered, and will be used to model appropriate Bingham distributions. The samples no. 1 (Tamanduá) and no. 2 (Águas Claras) are hard massive hematite ores with a granolepidoblastic fabric of partially oriented platy hematite crystals (specularite) included in granular hematite aggregates. Although the shape of both textures is similar the intensities of the crystallographic preferred orientation are different because of the different proportions of oriented specularite. The third sample from Andrade constitutes only of well-aligned specularite plates.

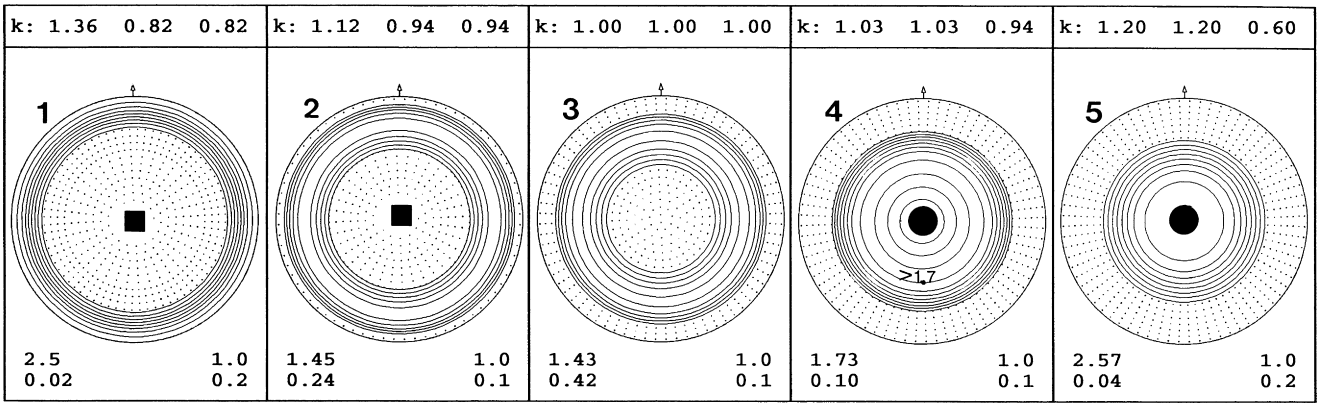

(a)

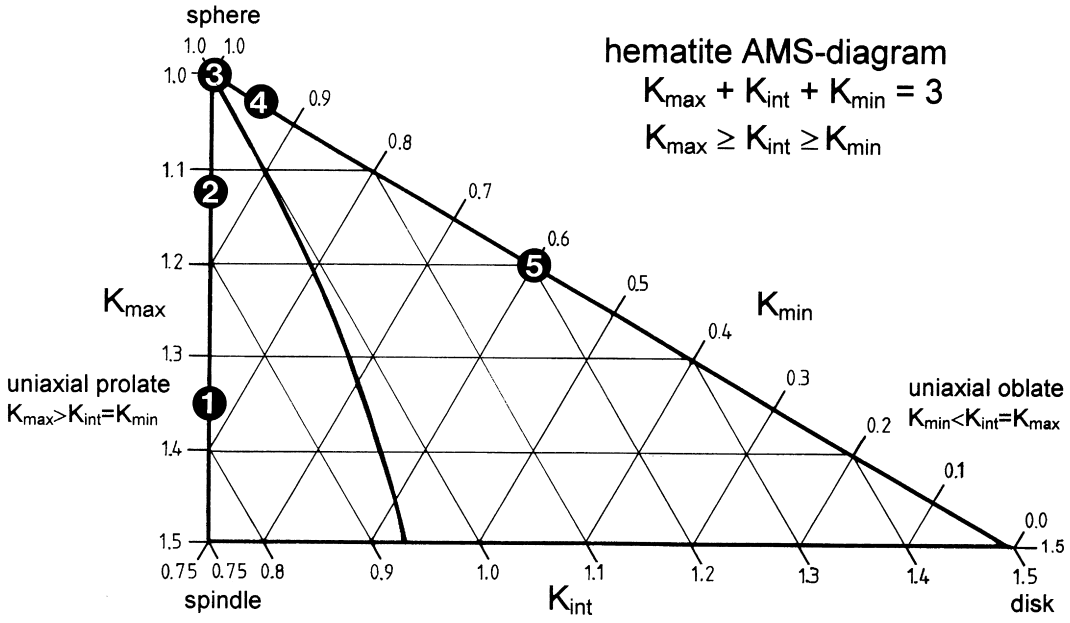

(b)

Fig. 6. Basal plane pole figures mathematically modeled by varying the parameters of the Bingham–Mardia distribution: (a) pole figures no. 1–5: $z = 5.0$, $\nu =$ 0.0, 0.4, 0.54, 0.8, 1.0; (b) location of the mathematical Bingham–Mardia pole figures in the AMS-diagram.

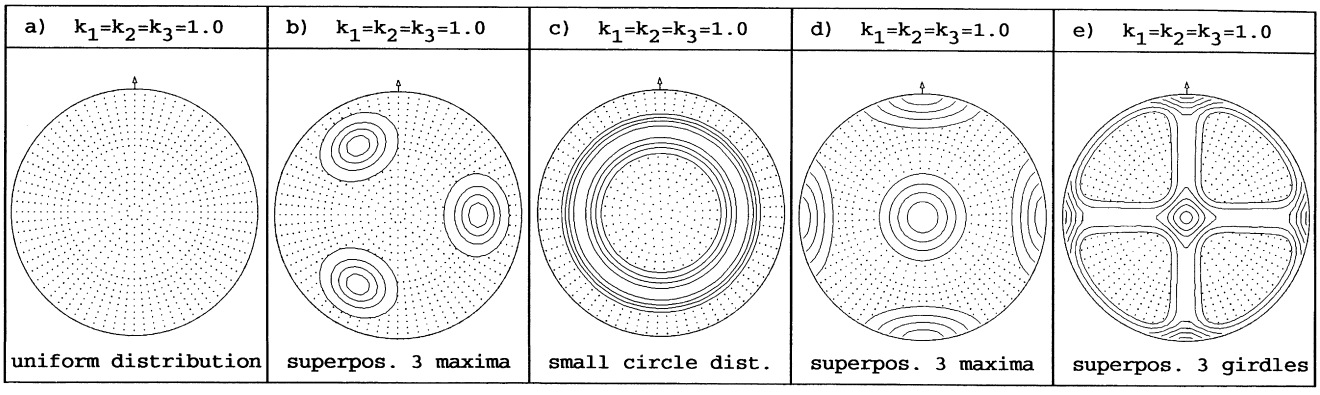

Fig. 7. Basal plane pole figures modeled by means of the Bingham distribution, the Bingham-Mardia distribution and superposition of three Bingham distributions, all with $K_{max} = K_{int} = K_{min} = 1.0$.

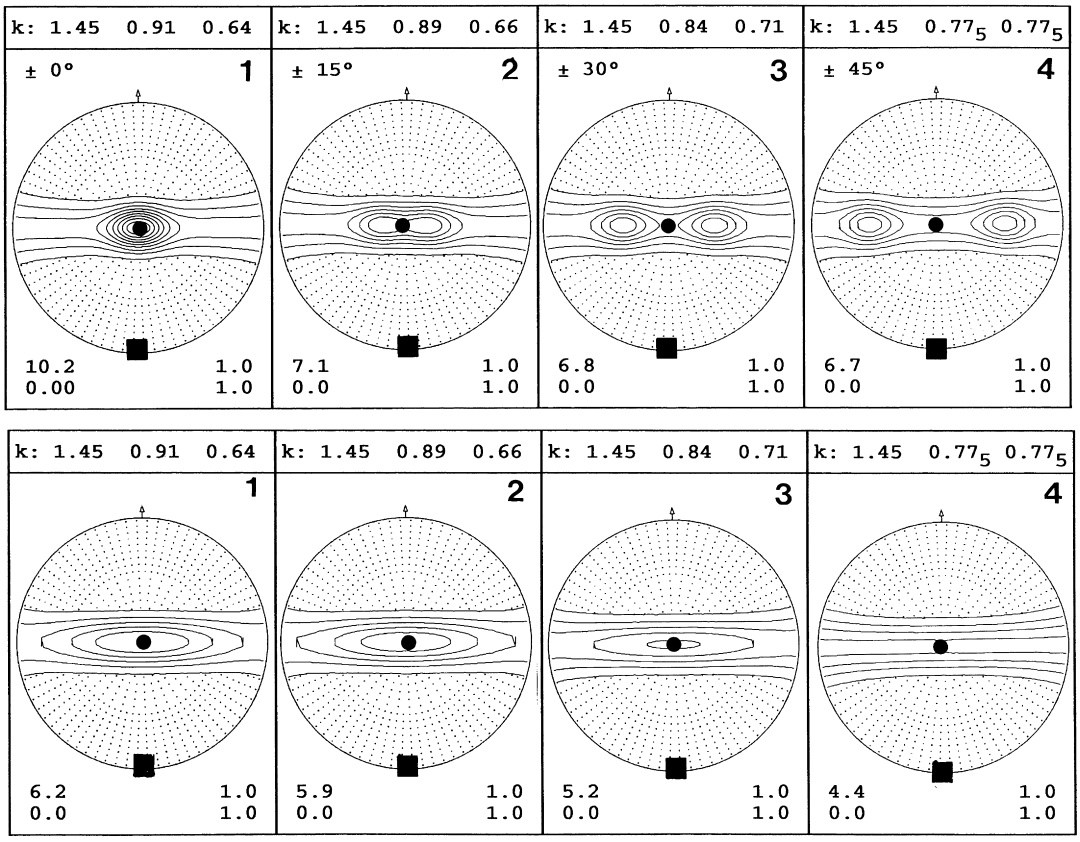

(a)

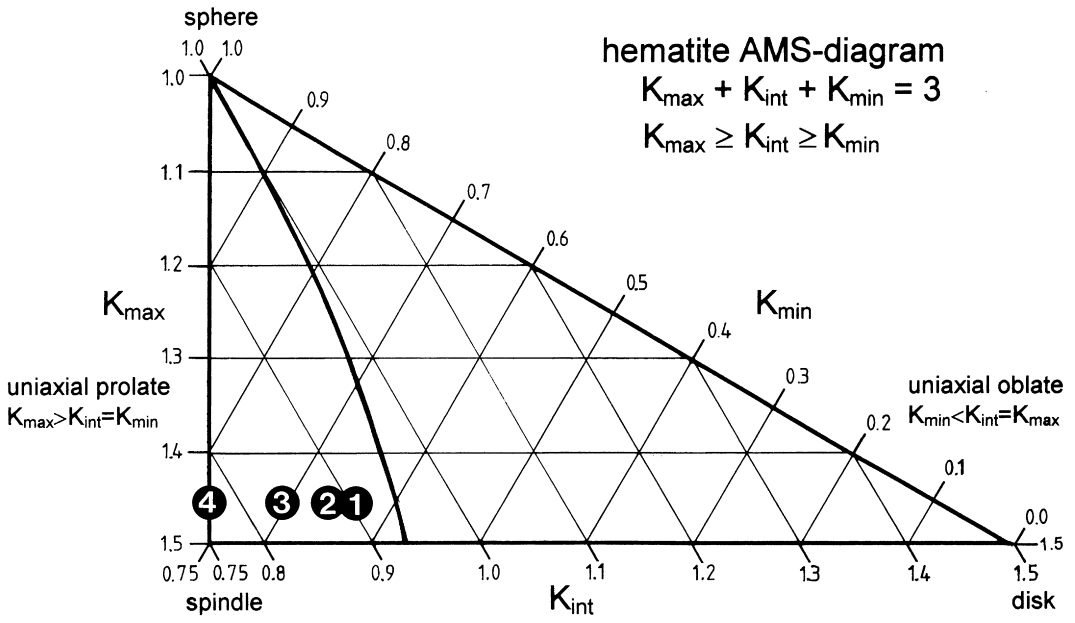

(b)

Fig. 8. Basal plane pole figures modeled Bingham distributions and varying its parameters. (a) Upper row: pole figures of three superposed Bingham distributions, where the maxima lie on the great circle in different symmetric positions to the center of the projection; lower row: pole figures of a single Bingham distribution with the same principal susceptibilities and identical position of the principal axes. (b) Location of these mathematical pole figures in the hematite AMS-diagram.

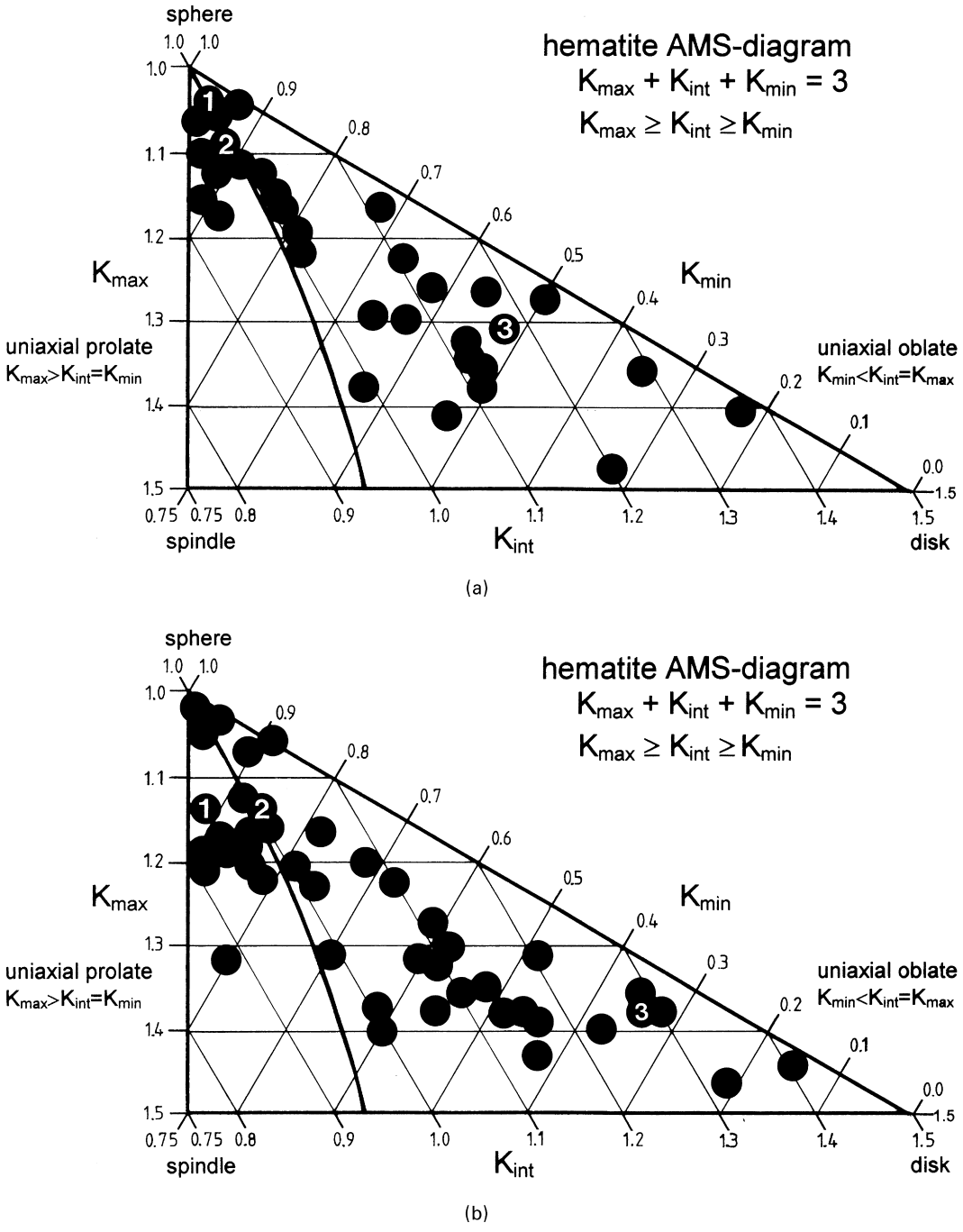

Fig. 9. Location of 44 samples from 10 mines of the Quadrilátero Ferrífero in the hematite AMS-diagram: (a) measured susceptibilities; (b) calculated susceptibilities from (003) neutron pole figures.

Specularitic ores of this type represent end members of originally mylonitic ore types where hematite is completely recrystallized and any rest of magnetite totally oxidized (Rosière et al., 1998, 1999). The first empirical fit has been performed to achieve approximately the same calculated susceptibilities for the experimental pole figures (Fig. 10, upper row) and for the mathematical pole figures (Fig. 10, lower row). For the first two samples (Tamanduá, Águas Claras) the fit seems reasonably good in relation to the orientation, shape as well as maximum and minimum densities. For the third sample from Andrade the difference in shape and especially in the maximum density is not acceptable. On the other hand the fit of a Bingham distribution to achieve conformity for the maximum density (Fig. 11) results in large differences of the susceptibilities. In order to fulfill both conditions a further attempt was successful using two different Bingham distributions (Fig. 12a, no.1 and 2). The superposition results in a very good

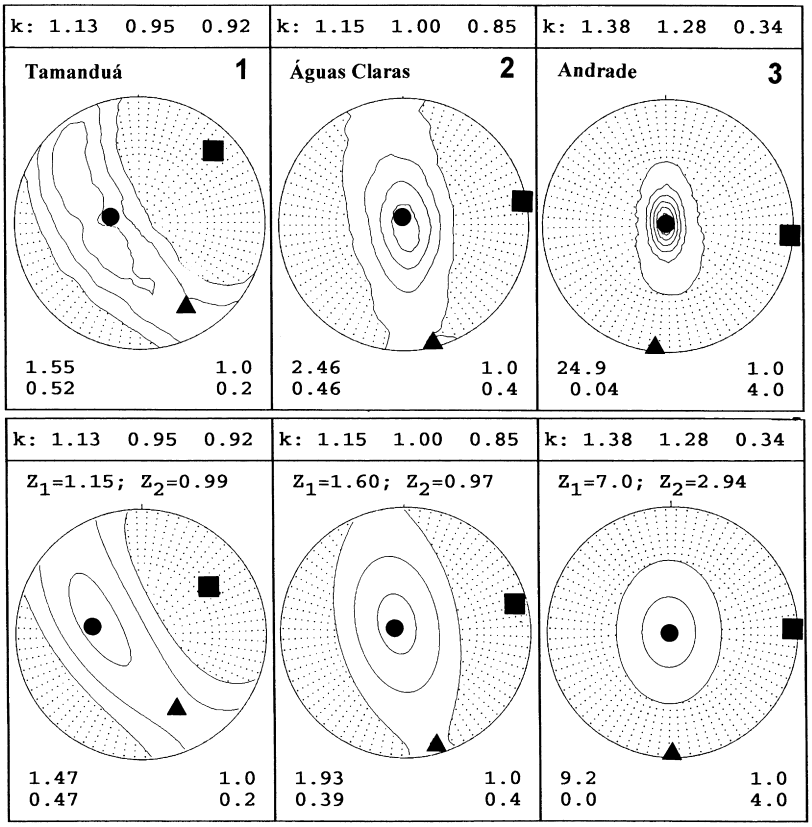

Fig. 10. Pole figures with susceptibilities axes of three samples from the Tamanduá-Mine (no. 1), Águas Clara Mine (no. 2) and the Andrade Mine (no. 3). Upper row: measured (003)-pole figures with their calculated susceptibilities; lower row: mathematical pole figures with their Bingham parameters modeled to fit approximately the same susceptibilities.

correspondence between the mathematical (Fig. 12a, no. s) and the measured (Fig. 12a, no. m) (003)-pole figure. The position of the measured, calculated susceptibilities, and its components in the AMS-diagram are shown in Fig. 12(b). In spite of these distinct differences between measured and calculated susceptibilities the principal axes are occupying approximately the same orientation as presented in the measured (003)-pole figure (Fig. 13).

The differences found between the measured and calculated susceptibilities are due to the fact that the calculated values refer to an ideal fabric with hematite point grains whereas the measured values reflect the three-dimensional real fabric with anisometric specularitic grain shapes, a grain size distribution, and grain size layering. The microscopic studies and the neutron and X-ray diffraction analysis of the three samples did not indicate any other accessory

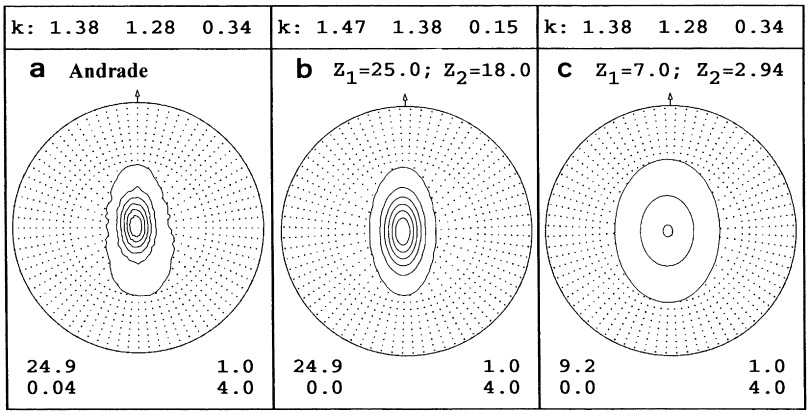

Fig. 11. Comparison of measured and modeled pole figures of the sample from the Andrade Mine: (a) measured pole figure; (b) fitted pole figure to meet the same densities; (c) fitted pole figure to meet the same susceptibilities.

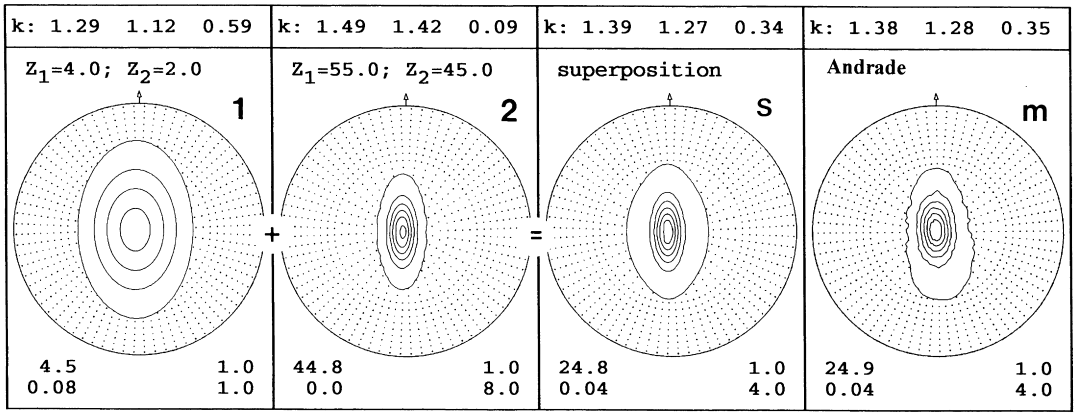

(a)

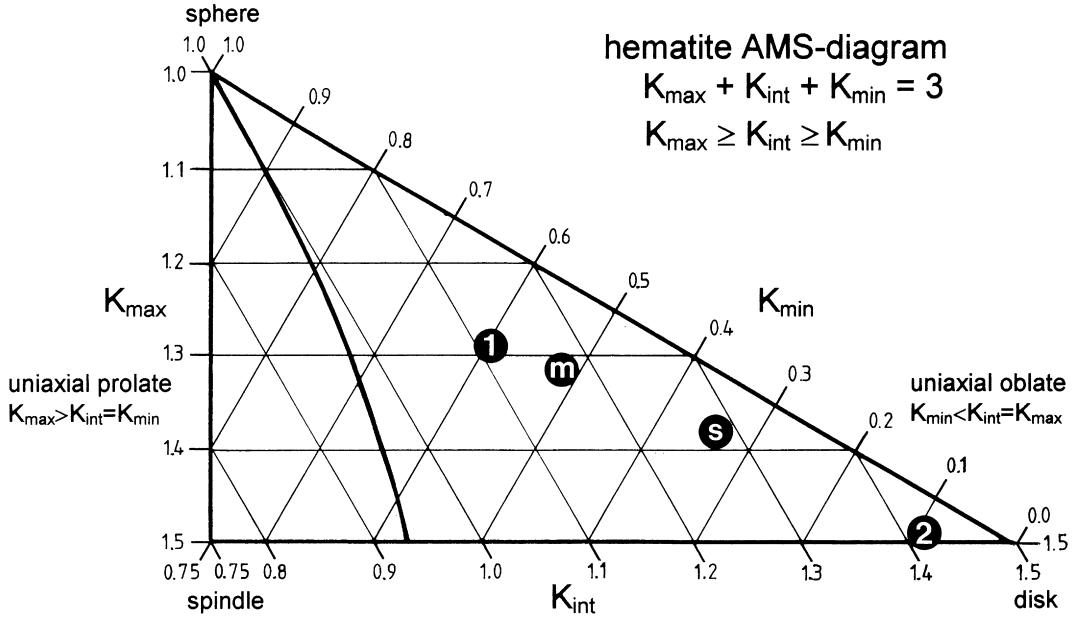

(b)

Fig. 12. Comparison of measured and modeled pole figures of the sample from the Andrade Mine. (a) Pole figure no. 1 is the first component for the superposition, no. 2 the second component, no. s shows the superposition of the two components meeting nearly the same susceptibilities, the same maximum and minimum densities and no. m is the measured pole figure for comparison. (b) AMS-diagram with the locations of the measured and superposed susceptibility values for the sample, and the susceptibilities of the two components used in the superposed mathematical model.

magnetic minerals. In order to get knowledge of the influence of trace minerals on the AMS measurement more sensitive analytical techniques have to be employed.

5. Conclusions

c-Axis pole figures of hematite ores reveal approximately circular, to elliptical, to great circle configurations. They are favorably modeled by means of the versatile Bingham distribution.

A wide variety of configurations has been modeled by varying the parameters of the Bingham distribution in order to visualize the relationship between *c*-axis distributions of hematite ores and calculated susceptibilities.

They reveal that quite different *c*-axis patterns of hematite ores may have the same magnetic parameters.

The crystallographic preferred orientation of the *c*-axes of hematite ores is strongly related to the foliation and lineation of ores. The pole of the foliation is centered at the *c*-axis maximum. The lineation is oriented perpendicular to the long axis of the elliptical *c*-axis maximum or perpendicular to the *c*-axis great circle.

The calculated principal susceptibilities are determined by the *c*-axis crystallographic preferred orientation. The minimum susceptibility is centered at the *c*-axis maximum

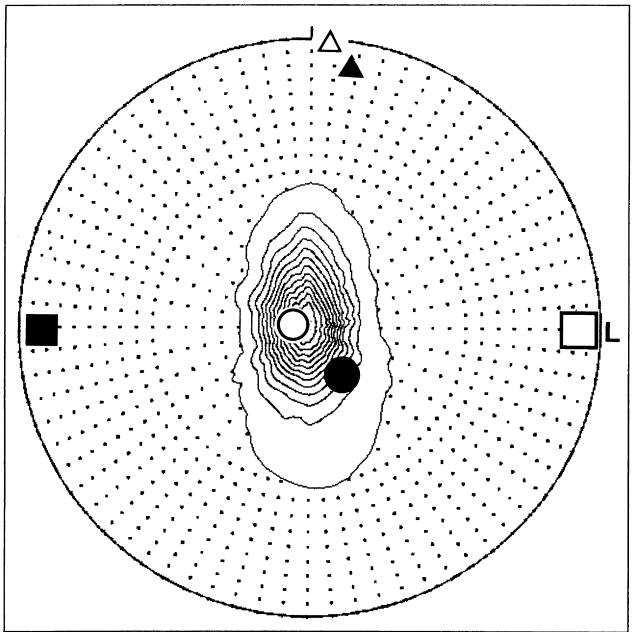

AMS	calculated	measured	difference
K_{max}	1.38	1.32	+0.06
K_{int}	1.28	1.16	+0.12
K_{min}	0.34	0.52	- 0.18

Fig. 13. Neutron measured (003)-pole figure of sample from the Andrade Mine with the orientation of the measured (closed symbols) and calculated (open symbols) principal susceptibility axes and the lineation L.

and the maximum susceptibility is centered at the maximum of the prism planes.

There might be a difference in the relative positions of measured and calculated principal susceptibilities with reference to the foliation poles and lineations. However, in general the direction of the maximum susceptibility is parallel to the lineation and the position of the minimum susceptibility corresponds to the pole of the foliation plane.

Determination of the magnetic anisotropy data is a valuable tool in the structural investigations of the fabric and the preferred orientation of hematite ores, but this rather inexpensive and fast magnetic method must be accompanied by the more expensive but unambiguous determination of preferred orientation by X-ray and neutron diffraction experiments in order to accomplish a complete and sound interpretation.

Acknowledgements

Thanks are due to H.-G. Brokmeier and E.M. Jansen for the neutron measurements of the hematite textures at the Forschungszentrum Geesthacht and W. Schäfer and E. Jansen at the Forschungszentrum Jülich. Financial support by the PROBRAL (CAPES/DAAD)- and FINEP/PADCT project 'Texture, physical anisotropy and metallurgy of iron ores of the Iron Quadrangle (Minas Gerais, Brazil)' is gratefully acknowledged. Financial support by the DFG permitted the presentation of preliminary versions of this contribution at the VI-SNET in Pirenópolis (GO), Brazil and at the ICOTOM-12 in Montreal, Canada. The referees are thanked for their helpful criticism and comments.

Appendix A. The Bingham distribution (Bingham, 1974)

The Bingham distribution for the unit sphere $\mathbf{S}^3$ in 3d Euclidean space $\mathbf{IR}^3$ is given by $f(\mathrm{x};\mathbf{a}_1,\mathbf{a}_2,\mathbf{a}_3,z_1,z_2,z_3) = \boldsymbol{C}(z_1,z_2,z_3)\exp(\Sigma z_i(\mathbf{a}_i\mathrm{x})^2)$, x, $\mathbf{a}_i \in \mathbf{S}^3 \subset \mathbf{IR}^3$. Apparently, it depends on three mutually orthonormal locations $\mathbf{a}_i \in \mathbf{S}^3$, $i = 1,2,3$, and three shape parameters z_i with respect to $\mathbf{a}_i$, $i = 1,2,3$. However, the latter are only determined up to an additive constant; thus, it is always possible to set one of the z_i equal to zero. The Bingham probability density function is an even function, i.e. $f(\mathrm{x};\mathbf{a}_1,\mathbf{a}_2,\mathbf{a}_3,z_1,z_2,z_3) = f(-\mathrm{x};\mathbf{a}_1,\mathbf{a}_2,\mathbf{a}_3,z_1,z_2,z_3)$. Therefore, it is appropriate to describe antipodally symmetric configurations of axes (lacking a directional sense). If two shape parameters, say z_1,z_2 are equal, then the distribution is rotationally symmetric with respect to the axis $\mathbf{a}_3$ corresponding to the remaining shape parameter z_3. If this remaining shape parameter z_3 is positive, then the axes (data) form two antipodally symmetric clusters around the corresponding localization parameter $\mathbf{a}_3$; if z_3 is negative, then the axes (data) form an antipodally symmetric girdle in the plane orthogonal to the corresponding localization parameter $\mathbf{a}_3$. Accordingly, if one of the shape parameters, say z_1, is much larger than the other two, which may be different, then the axes (data) form a cluster, which is not necessarily rotationally symmetric, with respect to its corresponding localization parameter $\mathbf{a}_1$; if two of the shape parameters, say z_1,z_2, which may be different, are much larger then the remaining one z_3, then the axes (data) form a girdle, which is not necessarily rotationally symmetric, with respect to its corresponding localization parameter $\mathbf{a}_3$.

Appendix B. The Bingham–Mardia distribution (Bingham and Mardia, 1978)

The Bingham–Mardia distribution for the unit sphere $\mathbf{S}^3$ in 3d Euclidean space $\mathbf{IR}^3$ is given by $f(\mathrm{x};\mathbf{a},z,\nu) = \mathrm{C}(z,\nu)\exp(-z(ax-\nu)^2)$, x, $\mathbf{a} \in \mathbf{S}^3 \subset \mathbf{IR}^3$. Apparently, it depends on one location parameter $\mathbf{a} \in$ S3 and two real shape parameters z, ν with respect to $\mathbf{a}$. For $\nu = 0$ it reduces to a special case of the Bingham distribution. If $0 < \nu < 1$, $z > 0$ the probability density function is maximum for all x^* with $\mathbf{a}x^* = \nu = \cos\ \theta$ and minimum in $x = \pm\mathbf{a}$. Thus, it refers to a small circle distribution in the plane orthogonal to $\mathbf{a}$ with an angle of aperture of arccos $\nu = \theta$. It should be noted that the Bingham–Mardia probability density function is not even. Therefore, it is appropriate to describe distributions of axes for sufficiently large z only.

References

Baars, F. J., Rosière, C. A., 1994. Geological map of the Quadrilátero Ferrífero. In: Baars, F. J., (1994). The São Francisco Craton. In: DeWitt, M. J., Ashwal, L. A. (Eds.), Greenstone Belts. Oxford Monographs on Geology and Geophysics Series, Oxford University Press, pp. 529-557.

Balsley, J.R., Buddington, A.F., 1960. Magnetic susceptibility anisotropy and fabric of some Adirondack granites and orthogneisses. American Journal of Science A258, 6–20.

Bingham, C., 1974. An antipodally symmetric distribution on the sphere. The Annals of Statistics 2, 1201–1225.

Bingham, C., Mardia, K.V., 1978. A small circle distribution on the sphere. Biometrika 65, 379–389.

Brokmeier, H.-G., 1989. Neutron diffraction texture analysis of multi-phase systems. Textures and Microstructures 10, 325–346.

Dorr, J. N. 2nd, 1969. Physiographic, stratigraphic and structural development of the Quadrilátero Ferrífero, Minas Gerais. United States Professional Paper, 641-A.

Ellwood, B.B., Hrouda, F., Wagner, J.-J., 1988. Symposia on magnetic fabrics: introductory comments. Physics of the Earth and Planetary Interiors 51, 249–252.

Hrouda, F., 1980. Magnetocrystalline anisotropy of rocks and massive ores: a mathematical model study and its fabric implications. Journal of Structural Geology 2, 459–462.

Hrouda, F., 1982. Magnetic anisotropy of rocks and its application in geology and geophysics. Geophysical Surveys 5, 27–62.

Hrouda, F., Siemes, H., Herres, N., Hennig-Michaeli, C., 1985. The relationship between the magnetic anisotropy and the c-axis fabric in a massive hematite ore. Journal of Geophysics 65, 174–182.

Jelínek, V., 1981. Characterization of the magnetic fabric of rocks. Tectonophysics 79, T63–T67.

Quade, H., Rosière, C. A., Siemes, H., Brokmeier, H.-G., 2000. Fabrics and textures of Precambrian iron ores from Brazilian deposits. Zeitschrift angewandte. Geologie Sonderheft 1, 155–162.

Rosière, C.A., Chemale Jr, F., 1991. Textural and structural aspects of iron ores from Iron Quadrangle, Brazil. In: Pagel, M., Leroy, J.L. (Eds.), Source, Transport and Deposition of Metals. Balkema, Rotterdam.

Rosière, C.A., Quade, H., Siemes, H., Chemale Jr., F., 1998. Fabric, texture and anisotropy of magnetic susceptibility in high-grade iron ores from the Quadrilátero Ferrífero, Minas Gerais, Brazil. Materials Science Forum, 273-275, 693-700.

Rosière, C.A., Siemes, H., Quade, H., Brokmeier, H.-G., Schaefer, W., Klingenberg, B., 1999. Deformação de formações ferríferas bandadas e a geração de especularita. Anais do VII Simpósio Nacional de Estudos Tectônicos (VII SNET). Lençóis (BA), Brazil, Sessão 5, pp. 31-34.

Siemes, H., Hennig-Michaeli, C., 1985. Ore Minerals. In: Wenk, H.-R. (Ed.). Preferred Orientation in Deformed Metals and Rocks, an Introduction to Modern Texture Analysis, Academic Press, Orlando, pp. 335–360.

Stacey, F.D., Joplin, G., Lindsay, J., 1960. Magnetic anisotropy and fabric of some foliated rocks from S.E. Australia. Geofisica pura e applicata 47, 30–40.

Wenk, H.-R., 1998. Typical textures in geological materials and ceramics. In: Kocks, U.F., Tomé, C.N., Wenk, H.-R. (Eds.), Texture and Anisotropy, Cambridge University Press, Cambridge, pp. 240–280.

Will, G., Merz, P., Schäfer, W., Dahms, M., 1990. Application of position sensitive detectors for neutron diffraction texture analysis of hematite ore. In: Barrett, C.S., Gilfrich, J.V., Huang, T.C., Jenkins, R., Predecki, P.K. (Eds.), Advances in X-Ray Analysis 33. Plenum Press, New York, pp. 277–283.

Will, G., Schäfer, W., Merz, P., 1989. Texture analysis by neutron diffraction using a linear position sensitive detector. Textures and Microstructures 10, 375–387.

Woodcock, N.H., 1977. Specification of fabric shapes using an eigenvalue method. Bulletin Geological Society of America 88, 1231–1236.